Catal Lett (2013) 143:267–275
DOI 10.1007/s10562-013-0963-0

Synthesis and Catalytic Performance of ZSM-5/MCM-41 Zeolites With Varying Mesopore Size by Surfactant-Directed Recrystallization

Jindan Na · Guozhu Liu · Tianyou Zhou · Guochang Ding · Shenlin Hu · Li Wang

Received: 10 September 2012 / Accepted: 17 January 2013 / Published online: 29 January 2013
© The Author(s) 2013. This article is published with open access at Springerlink.com

Abstract ZSM-5/MCM-41 zeolite composites with varying mesopore sizes were prepared through alkali-desilication and surfactant-directed recrystallization with different chain length of alkyltrimethylammonium bromide. XRD and TEM revealed that the composites possessed the characteristics of both ZSM-5 and mesoporous MCM-41 with hexagonal symmetry. N_2-adsorption–desorption, ^{27}Al MAS NMR, NH_3-TPD and in situ FT-IR results suggested that the sizes of the mesopores and the accessibility of acid sites could be affected greatly by the chain length of alkyltrimethylammonium bromide used. Catalytic cracking of *n*-dodecane over ZSM-5/MCM-41 composites was studied in the form of coatings on the inside of a tubular reactor at 550 °C and 4 MPa. The conversion of *n*-dodecane increased gradually with increasing the mesopore sizes of ZSM-5/MCM-41 composites, implying a positive effect of the mesopores on the diffusion inside pore channels and the accessibility of acid sites by the reactants.

Keywords ZSM-5/MCM-41 composite zeolites · Mesopore size · Recrystallization · Catalytic cracking · *n*-Dodecane

J. Na · G. Liu · T. Zhou · G. Ding · L. Wang (✉)
Key Laboratory of Green Chemical Technology of Ministry of Education, School of Chemical Engineering and Technology, Tianjin University, Tianjin 300072, China
e-mail: wlytj@tju.edu.cn

S. Hu
Science and Technology on Scramjet Laboratory, Beijing 100074, China

1 Introduction

Recently, an interest in the catalytic cracking of hydrocarbon fuels is motivated by the desire to enhance engine performance over the entire spectrum of flight regimes. For hypersonic flight, hydrocarbon fuels can serve as not only source of heat through combustion, but also coolant through the cracking reaction to remove waste heat from aircraft systems [1–5]. Huang et al. [1], Sobel and Spadaccini [6] and Sicard et al. [7] investigated the cracking of several fuels, including conventional kerosene-base jet fuels (JP-7, JP-8 and JP-8+100), *n*-heptane and Norpar 12 (a blended normal paraffin) in a zeolite-coated reactor under the simulated high-speed flight conditions (650 °C and 2.4 MPa). Fan et al. [8] studied the catalytic cracking of China No. 3 aviation kerosene over wall-coated HZSM-5 zeolite under conditions similar to the practical scramjet applications (777 °C and 7.0 MPa). Liu et al. [9, 10] studied the effects of the Si/Al ratio and crystal size (nano- and microscale) of ZSM-5 zeolites coated on the wall of a flowing tubular reactor on the cracking of *n*-dodecane at 550 °C and 4.0 MPa. The results indicated that HZSM-5 zeolite is an ideal candidate for the cracking of hydrocarbon fuels because of its relatively low coke deposition. However, the relatively small pore size of ZSM-5 zeolite limits the diffusion of bulky molecules from the surface to active sites located in the pores, which makes its catalytic activity being not fully exhibited. To overcome this limitation, one way is to shorten the diffusion length, and another way is to improve the effective diffusivity of the reactant molecules in the zeolite pores. For the latter strategy, micro-/mesopore composite zeolites with the strong acidity of micropore zeolites and the mesopores in the typical range of 2–15 nm have been intensively developed [11].

Pérez-Ramírez et al. [11], Čejka and Mintova [12] and Prokešová et al. [13] systematically summarized the development in the remarkably growing field of the synthesis, characterization and application of zeolite-based micro/mesoporous composites as catalysts in acid-catalyzed reactions, oxidation reactions and discussed the advantages and disadvantages of the synthesis approaches for the preparation of the micro/mesoporous composites in their review and research articles. Desilication by alkali treatment reported for the first time by Groen et al. [14–17] is an important and widely used methodology for the preparation of hierarchical zeolites of micro- and mesopores. Matsukata and co-workers [18] investigated the effects of alkali treatment parameters on the morphology and acidity of the ZSM-5 zeolite and the conversion of the cumene cracking, and found that mesopores created during desilication improved the adsorption and diffusion properties of cumene, resulting in the increase in the conversion of the cumene cracking. Seo and co-workers [19] modified ZSM-5 zeolites by a similar alkali treatment process and employed them as catalysts in the catalytic cracking of *n*-octane. The results showed that the low acidity and short residence time induced by alkali treatment resulted in the reduction of cracking conversion, but enhanced the selectivity to primary cracking products. Shen and co-workers [20] studied the relationship between the SiO_2/Al_2O_3 ratios and the catalytic activity of alkali-treated ZSM-5 zeolites, and found that the zeolite with the low SiO_2/Al_2O_3 ratios preserved the relatively complete crystal structure after alkali treatment and gave a higher yield of light olefins for the heavy oil cracking compared to the untreated zeolite.

A major problem often encountered during the creation of mesopores in micropore zeolite crystals by alkali treatment is the loss of crystallinity and acid sites, which causes the decrease in the catalytic performance. Pérez-Ramírez et al. [21] developed a novel desilication method involving NaOH treatment of ZSM-5 in the presence of quaternary ammonium cations which act as a pore-growth mediator, protecting the zeolite crystal during the demetallation process. The authors proposed that the category of the hierarchical porous zeolites could be quantitatively described using a parameter, namely hierarchy factor (HF) which is independent of the type and synthesis method, and gave a correlation between the catalytic activity in benzene alkylation and HF of the hierarchical porous ZSM-5.

Another alternative approach is recrystallization of the dissolved species in the presence of surfactants after desilication. Goto et al. [22] synthesized ZSM-5/MCM-41 composite zeolites using hexadecyltrimethylammonium chloride as templates in NaOH solution. The products showed strong acid sites like ZSM-5 and an increase in the cracking conversion of *n*-hexane. Qi et al. [23] studied the effect of recrystallization time on the morphology of the products. The parent ZSM-5 zeolite was dissolved and its structure was destroyed completely with prolonging crystallization time up to 72 h. The sample recrystallized for 12 h showed a high catalytic activity in 1,3,5-triisopropylbenzene cracking. Ying and co-workers [24] and Zhao and co-workers [25] synthesized ZSM-5@mesoporous silica composite zeolites using cetyltrimethylammonium bromide as templates under the alkaline reaction conditions. The composite materials possessed a core–shell structure and showed a higher cracking conversion of *n*-dodecane than the untreated HZSM-5. The authors concluded that the reason for high catalytic activity was due to the existence of mesoporous silica shells which can passivate the acid sites on the external surface of zeolites, thereby alleviating the formation of cokes. Stein et al. [26] synthesized ZSM-5 zeolites with mesopores through desilication and reassembly processes. They found that the physicochemical properties of the treated zeolites depended on the Si/Al ratios, the hydroxide concentration and the presence of surfactants.

The aim of this paper is to better understand the relationship between the catalytic activity and the pore structure of zeolites. Firstly, ZSM-5/MCM-41 composite zeolites were synthesized by sequential alkali-desilication and surfactant-directed recrystallization with alkyltrimethylammonium bromide as templates. The mesopore sizes of the composite zeolites were manipulated by changing the chain length of alkyltrimethylammonium bromide (C_nTAB, $n = 10$, 12, 14 and 16). Secondly, physicochemical properties of the ZSM-5/MCM-41 composite zeolites were characterized by X-ray powder diffraction (XRD), nitrogen adsorption–desorption measurements, transmission electron microscopy, pyridine-adsorbed Fourier transform-infrared spectroscopy, ammonia temperature-programmed desorption, inductively coupled plasma atomic emission spectroscopy and ^{27}Al solid-state magic-angle-spinning nuclear magnetic resonance spectra. Finally, the catalytic cracking of supercritical *n*-dodecane was carried out in a flowing tubular reactor with wall-coated by ZSM-5/MCM-41 composite zeolites at 550 °C and 4 MPa.

2 Experimental

2.1 Materials

The HZSM-5 zeolite (SiO_2/Al_2O_3 molar ratio of 107) with the average crystal sizes of 3–4 μm was purchased from the Novel Chemical Corporation (Shanghai, China). Decyltrimethylammonium bromide ($C_{10}TAB$), dodecyltrimethylammonium bromide ($C_{12}TAB$), tetradecyltrimethylammonium bromide ($C_{14}TAB$) and cetyltrimethylammonium bromide ($C_{16}TAB$) were purchased from J&K

Chemical Ltd without further purification. *n*-Dodecane with 99.5 % purity was obtained from Sinopharm Chemical Reagent Co., Ltd (Shanghai, China).

2.2 Synthesis of ZSM-5/MCM-41 Composite Zeolites

ZSM-5/MCM-41 composite zeolites were prepared via the surfactant-directed recrystallization process using alkyltrimethylammonium bromide with various chain lengths (C_nTAB, $n = 10$, 12, 14 and 16) as templates. In a typical run, 0.5 g HZSM-5 was added to 1.5 M sodium hydroxide aqueous solution (5 mL) and then the mixture was stirred for 30 min at room temperature. 10 g aqueous solution of alkyltrimethylammonium (10 wt%) was added to the suspension, followed by an additional stirring for 30 min. Then the mixture was transferred to a Teflon-lined autoclave and hydrothermally treated at 120 °C for 12 h. After cooling to room temperature, the pH value of the reaction mixture was adjusted to 8.5 by dropwise addition of 2.0 M HCl under vigorous stirring. The mixture was transferred into the Teflon-lined autoclave and heated at 120 °C for 24 h. Finally, the product was recovered by centrifugation, washed repeatedly with deionized water and dried at 100 °C overnight. The resulting powder was calcined at 550 °C for 6 h to remove the surfactant.

The protonated form of the samples was obtained by repeated ion-exchange with 1.0 M NH_4NO_3 solution at 90 °C for 4 h and calcination at 550 °C for 4 h. The samples synthesized with C_{10}TAB, C_{12}TAB, C_{14}TAB and C_{16}TAB are denoted as HZM-C10, HZM-C12, HZM-C14 and HZM-C16, respectively. The sample without further recrystallization process after desilication with the sodium hydroxide solution is denoted as AT-ZSM-5.

2.3 Characterization

XRD measurements were carried out using a Philips X'Pert MPD diffractometer equipped with Cu–Kα radiation (40 kV, 200 mA for wide angle patterns and 100 mA for small angle patterns). Transmission electron microscope (TEM) images were obtained using a JEM-2100F microscope. Nitrogen adsorption–desorption measurements were carried out at 77 K using a Micromeritics ASAP 2020 volumetric adsorption analyzer. Samples were degassed at 300 °C for 24 h prior to the exposure to nitrogen gas. The Brunauer–Emmett–Teller (BET) method was applied to estimate specific surface area. Micropore volumes were determined using the *t* plot method. The pore size distribution was calculated by the Horvath-Kawazoe (HK) model and Barrett–Joyner–Halenda (BJH) model using desorption branch of the isotherm. Ammonia temperature-programmed desorption (NH_3-TPD) were measured on a Quantachrome CHEMBET 3000. The samples of 0.0500 g were charged in a quartz tubular reactor and pretreated at 600 °C with an Ar flow of 30 mL min^{-1} for 1 h and then cooled to 50 °C. Ammonia (20 % NH_3 in He) was introduced at a flow rate of 30 mL min^{-1} for 0.5 h at 50 °C and then a He stream was fed in until a constant TCD signal was obtained. The physisorbed ammonia was removed by flowing He for 60 min at 100 °C. The chemically adsorbed ammonia was determined by rising the temperature up to 600 °C with a heating rate of 10 °C min^{-1}. Solid-state ^{27}Al magic-angle-spinning nuclear magnetic resonance (^{27}Al MAS NMR) spectra were measured on a Bruker AV300 using a frequency of 78.2 MHz with a spin rate of 8.0 kHz. The pulse length of 0.5 μs with a pulse delay of 1.0 s was adopted. Pyridine-adsorbed infrared spectroscopy (Py-IR) was recorded on a FT-IR Bruker Equinox spectrometer. The powder samples were pressed to self-supported wafers (ca. 10 mg cm^{-2}) and treated directly in an in situ IR cell connected to a vacuum adsorption apparatus allowing to obtain a residual pressure below 10^{-3} Pa. Adsorption of pyridine (or 2,4,6-trimethylpyridine) proceeded at 60 °C for 30 min, followed by desorption at 300 °C for 20 min. Then, IR spectra were recorded with a resolution of 2 cm^{-1} by collecting 45 scans for a single spectrum. Silicon and aluminum contents of the zeolites were determined using an inductively coupled plasma (ICP) spectroscopy (USA Thermo Jarrell-Ash Corp. ICP-9000(N+M)).

2.4 Catalytic Cracking of *n*-Dodecane

The catalytic cracking of *n*-dodecane was carried out in a flowing reactor with catalyst coatings consisting of the HZM series, AT-ZSM-5 and HZSM-5 zeolite, as described in our previous works [3, 9, 10, 27]. The reactor was 304 stainless-steel tubes with 300 mm in length, 3 mm in outside diameter and 0.5 mm in wall thickness. A washcoating method was used for the preparation of the zeolite coatings on the inner surface of the reactor. The same compositions and conditions were used to obtain the close loading amounts of zeolites and thickness of coatings. The solid (zeolite:inert binder = 1:1.5) loading amount was 4.200 ± 0.200 mg cm^{-2} and the coating thickness was 22.2 ± 0.3 μm. The reactor was heated by direct current power and its wall temperature was measured by K-type thermocouples. The pressure was maintained at 4 MPa by a backpressure valve. The flow rate of *n*-dodecane in inlet of the reactor was controlled by a high-pressure liquid chromatography pump and kept at 10 mL min^{-1}. The reaction products were cooled first by a condenser and then flowed into a gas–liquid separator. The liquid products were analyzed by a HP4890 gas chromatography with an FID and a PONA column (50 m × 0.53 mm). Each sample was collected in 5 min to ensure enough weight of gas and liquid samples for the material balance. For each zeolite catalyst

tested, two individual runs were performed to ensure the reproducibility of the experimental results. The conversion of *n*-dodecane was calculated as follows:

$$X_{n-\text{dodecane}} = \frac{W_{n-\text{dodecane,in}} - W_{n-\text{dodecane,out}}}{W_{n-\text{dodecane}}}$$

where $W_{\text{n-dodecane,in}}$ and $W_{\text{n-dodecane,out}}$ were the mass of *n*-dodecane in inlet and outlet of the reactor, respectively.

Cokes on the wall of the reactor were analyzed by the temperature-programmed oxidation (TPO) method, according to Meng et al. [3].

3 Results and Discussion

3.1 XRD

Figure 1 shows the XRD patterns of AT-ZSM-5 and ZSM-5/MCM-41 zeolites (HZMs). In the small angle diffraction range (Fig. 1a), there were three diffraction peaks at $2\theta = 2.3$, 4.2 and 4.8°, attributed to the (100), (110) and (210) crystal faces of long-range ordered hexagonal MCM-41 for the HZM samples. However, for AT-ZSM-5 there were no characteristic peaks of MCM-41 being observed. The results indicated that the surfactant-directed recrystallization after alkali treatment led to the formation of mesporous MCM-41. Moreover, it could be found that the intensity of peaks at $2\theta = 2.3°$ for HZMs increased and the position of this peak shifted to low angle continuously with increasing the alkyl chain length in alkyltrimethylammonium used. In the wide angle diffraction range (Fig. 1b), there were two diffraction peaks between $2\theta = 7$ and 10° and three diffraction peaks between $2\theta = 22.5$ and 25°, attributed to the (110), (020), (501), (151) and (303) crystal faces, respectively, which are the characteristic diffraction peaks of the MFI zeolite.

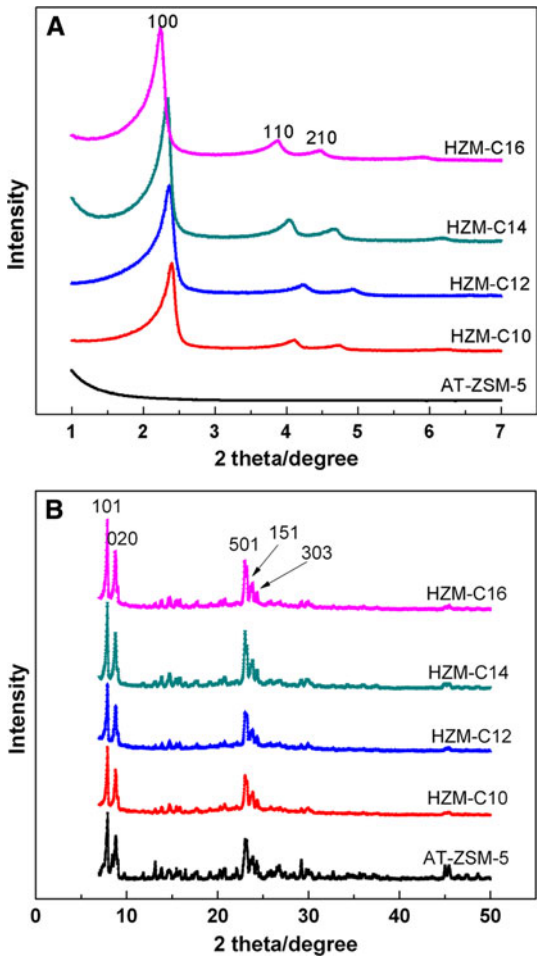

Fig. 1 **a** Small angle XRD patterns. **b** Wide angle XRD patterns of the AT-ZSM-5 and ZSM-5/MCM-41 composite zeolites

3.2 N_2 Adsorption–Desorption

Figure 2 illustrates the N_2 adsorption–desorption isotherms and the pore size distribution curves of ZSM-5, AT-ZSM-5 and ZSM-5/MCM-41 zeolites. The corresponding textural properties are summarized in Table 1. As shown in Fig. 2a, the untreated ZSM-5 displayed typical type I isotherms with a sharp uptake at low relative pressure and then an constant amount of N_2 adsorbed at the relative pressure up to one, demonstrating a characteristic microporous framework. Although the adsorbed amount of N_2 increased slightly, the isotherm of AT-ZSM-5 changed characteristically from type I to type IV, suggesting the creation of mesopores in AT-ZSM-5 sample. All ZSM-5/MCM-41 composite zeolites showed typical type I isotherms at the relative pressure below 0.02 and type IV isotherms with a capillary condensation loop in the range of $P/P_0 = 0.5$–1.0, indicating the presence of mesoporous phase. It was worth noting that steep and small hysteresis loops at relative pressure P/P_0 ranging from 0.25 to 0.4 existed in the isotherms of HZM-C14 and HZM-C16. The hysteresis loops at low P/P_0 were also observed in the isotherms of hierarchical ZSM-5 zeolites by Dou and co-workers [28], Xu and co-workers [29] and Čejka and co-workers [30] and were attributed to the commencement of pore filling, characteristics of a mesoporous material with a narrow pore size distribution above 3 nm [31, 32]. As shown in Fig. 2c, HZM-C14 and HZM-C16 exhibited mesopores with the pore size centered on 3.2 and 3.8 nm, respectively, whereas HZM-C10, HZM-C12 and AT-ZSM-5 exhibited mesopores with the pore size below 3 nm, supporting the speculations mentioned above. The mesopores ranging from 4.0 to 5.0 nm for all HZMs were due to the presence of secondary pores associated with the voids between the individual nanounits.

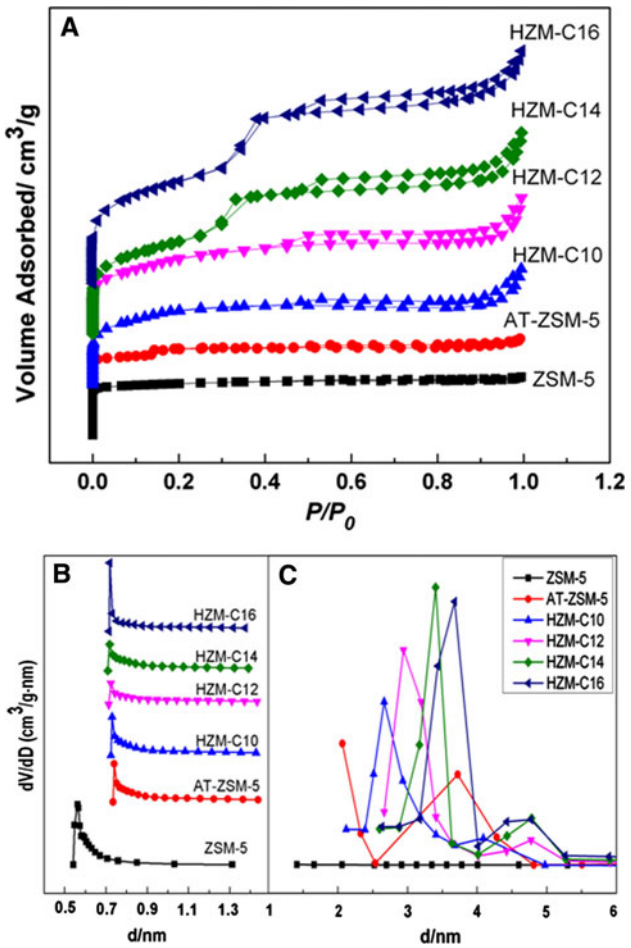

Fig. 2 N_2 adsorption–desorption isotherms (**a**), micropore size (**b**) and mesopore size (**c**) distribution of ZSM-5, AT-ZSM-5 and ZSM-5/MCM-41 composites

We noted another two phenomena in Fig. 2b, c. One is that all the treated samples showed almost the same micropore size distributions centered around 0.8 nm, which was larger than that of the untreated ZSM-5. Kokotailo and Rohrman [32] and Sulikowski and co-workers [33] found that alkali treatment led to the "cleaning" of the ZSM-5 zeolite channels by dissolving very small contaminations. Therefore, the enlargement of the micropore size of HZMs might be caused by the dissolution of pore wall during alkali treatment and cleaning effect of NaOH solution. The other phenomenon is that the mesopore size of AT-ZSM-5 was smaller than that obtained by Serrano et al. [30] whose sample prepared by alkali treatment showed about 10 nm in the pore size. The difference in the sizes of mesopores between the two samples was possibly caused by the different treatment conditions, i.e. 90 °C and 20 h were used by Serrano et al. [30], whereas room temperature and 0.5 h were used in this work.

From Table 1, it can be seen that there was a steep and continuous increase in both the specific surface area and mesopore volume of HZMs with the chain length of surfactants compared to that of AT-ZSM-5, suggesting that recrystallization after NaOH treatment was beneficial to the formation of mesopores. But, no discernable difference in the micropore volumes was observed for all the treated zeolites. According to the formation mechanisms of MCM-41 described by Beck et al. [34], Kresge et al. [35] and Zhao et al. [25], the cationic surfactant molecules interact with the negatively charged zeolite surface to form surface micelles, and then the hydrolytic condensation of silicate species dissolved from zeolite crystals due to the alkalinity of NaOH solution proceed to the formation of mesopore phase around the micelles. Apparently, the chain length of surfactants determines the sizes of the surface micelles, resulting in the difference in the sizes of mesopores.

3.3 TEM

From Fig. 3a, only straight channels with the pore diameter of around 0.6 nm were found in the untreated ZSM-5. After the treatment with NaOH solution, the irregular voids distributed randomly in the interior of the crystals were observed (Fig. 3b), indicating the existence of irregular mesopores in AT-ZSM-5 crystals, which was consistent with its broad size distribution of mesopores. For the ZSM-5/MCM-41 composite zeolites (Fig. 3c–f), there were two types of pore structures, corresponding to crystalline micropore and ordered hexagonal mesopore, respectively, and a clear interface between the micropores and mesopores existed. The shell-like mesopore phase covered the crystalline micropore crystal, i.e. the core–shell structure

Table 1 Physical properties of ZSM-5, AT-ZSM-5 and ZSM-5/MCM-41

Sample	S_{BET} (m^2/g)	S_{exter} (m^2/g)	V_{meso} (cm^3/g)	V_{micro} (cm^3/g)	Pore diameter (d/nm)	
					Micropore	Mesopore
ZSM-5	370	69	0.05	0.14	0.63	–
AT-ZSM-5	393	276	0.15	0.05	0.82	1.92
HZM-C10	539	359	0.29	0.08	0.83	2.68
HZM-C12	550	443	0.37	0.05	0.83	3.08
HZM-C14	669	540	0.57	0.05	0.83	3.73
HZM-C16	739	610	0.66	0.05	0.84	3.90

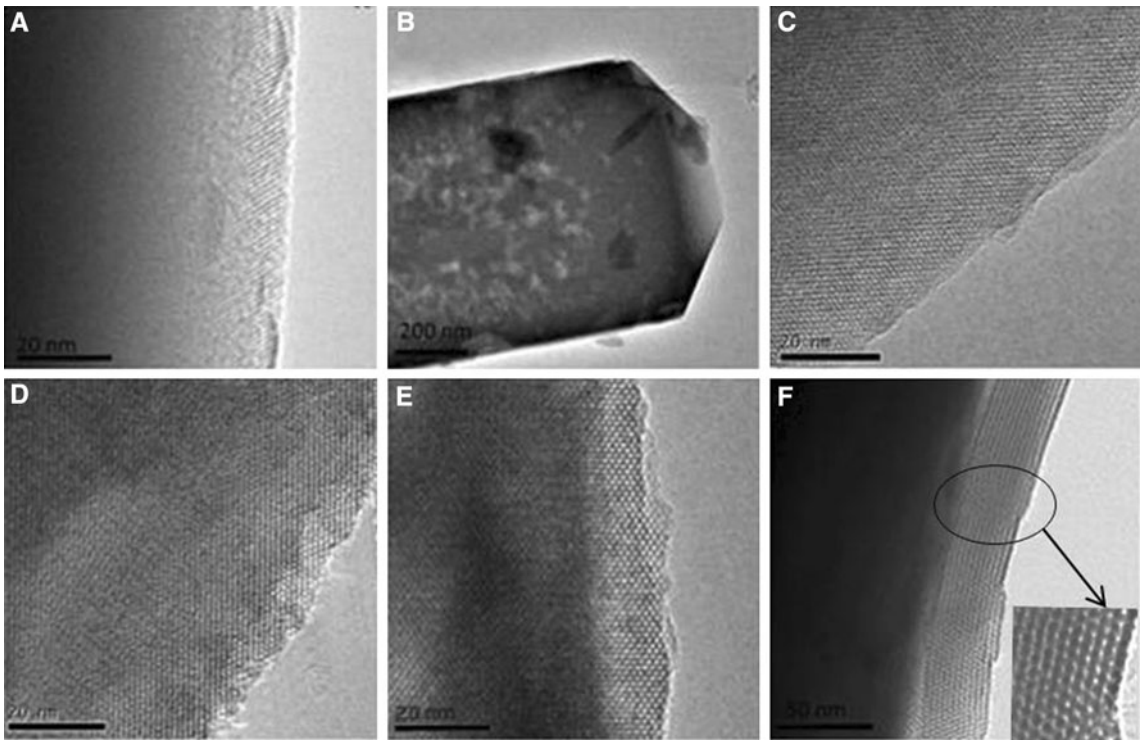

Fig. 3 TEM images of ZSM-5 (**a**), AT-ZSM-5 (**b**), HZM-C10 (**c**), HZM-C12 (**d**), HZM-C14 (**e**) and HZM-C16 (**f**)

formed. The thickness and uniformity of the mesopore shells increased with the chain length of CTAB.

3.4 ^{27}Al NMR Spectroscopy

^{27}Al MAS NMR spectra of ZSM-5, AT-ZSM-5 and HZM-C14 are shown in Fig. 4. As seen, there were two main peaks in ^{27}Al MAS NMR spectra for the three samples, which had similar total Si/Al ratios (ca. 50) measured by ICP. The one at 59 ppm could be assigned to the tetrahedral framework Al species, and the other at 0 ppm could be attributed to the octahedral extra-framework Al species [36]. The ratios of framework Al to extra-framework Al were calculated from the integral area of the two main peaks and the values were: 9.03 for the untreated ZSM-5, 2.21 for AT-ZSM-5 and 3.09 for HZM-C14, indicating the loss of framework Al species from AT-ZSM-5 to a higher extent than that from HZM-C14. These results suggested that the surfactant-directed recrystallization process was helpful for incorporating Al species dissolved during alkali treatment from zeolites into framework of zeolites again.

3.5 NH_3-TPD

Figure 5 presents NH_3-TPD results. For all samples, there were two desorption peaks at 190–220 °C and 380–420 °C, corresponding to the weak and strong acid sites, respectively. The intensities of both peaks for AT-ZSM-5 and

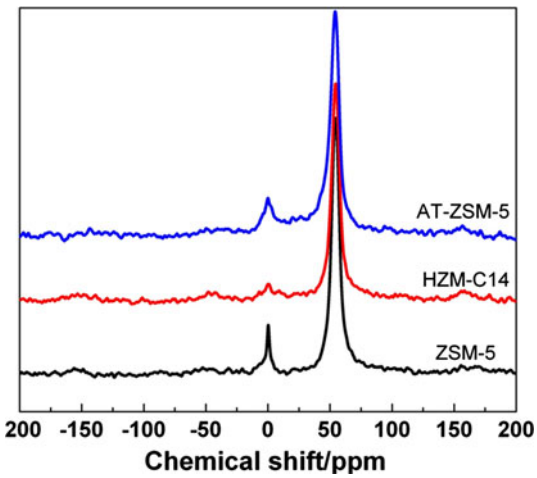

Fig. 4 ^{27}Al MAS NMR spectra of ZSM-5, HZM-C14 and AT-ZSM-5

ZSM-5/MCM-41 composite zeolites were weaker than that for the untreated ZSM-5, indicating the decrease in the amount of acid sites. Among all the samples, AT-ZSM-5 gave the lowest amount of total acid sites, while the untreated ZSM-5 gave the highest. HZMs had the moderate amount of total acid sites with the ratios of weak to strong acid sites similar to that of AT-ZSM-5. As shown in Fig. 5, there were no discernable difference in the maximum temperature of both peaks among the five treated samples, suggesting the close strength of acid sites for AT-ZSM-5

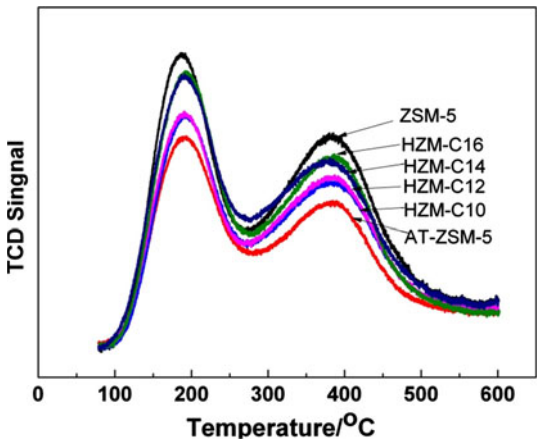

Fig. 5 NH_3-TPD profiles of ZSM-5, AT-ZSM-5 and HZM series

and HZMs. Matsukata and co-workers [18] measured the concentrations of Si and Al dissolved from ZSM-5 during alkali treatment and demonstrated that dealuminization accompanying with desilication occurred during alkali treatment. Similar results were also observed by Xu and co-workers [29] and Groen and co-workers [36, 37], Groen et al. [37]. Therefore, it could be assumed that the decreases in the amount of acid sites for AT-ZSM-5 and HZMs were caused by dealuminization, whereas the higher amount of acid sites for HZMs than for AT-ZSM-5 was because of the partial recovery of acid sites during recrystallization process in which the Al species dissolved during alkali treatment incorporated again into the framework of zeolites.

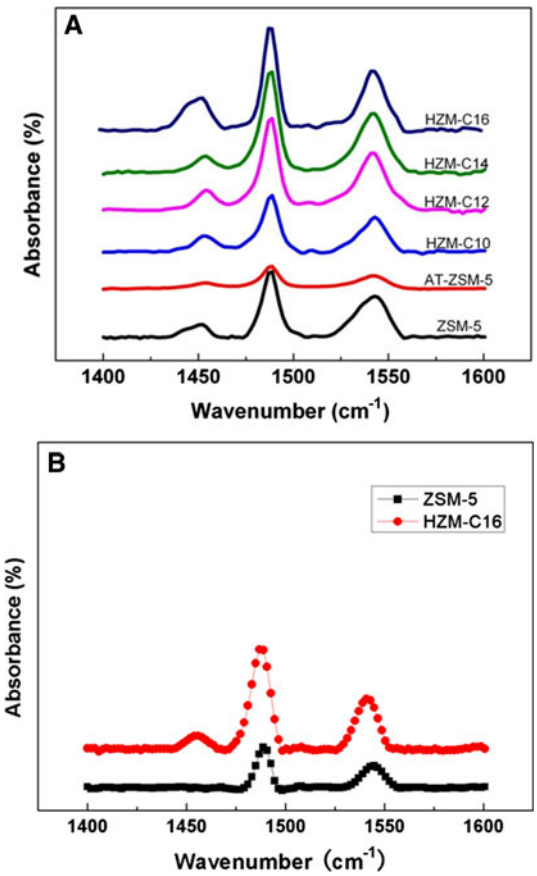

Fig. 6 Pyridine-adsorbed IR spectra of ZSM-5, AT-ZSM-5 and HZM series (**a**) and 2,4,6-trimethyl pyridine-adsorbed IR spectra of ZSM-5 and HZM-C16 (**b**)

3.6 Pyridine-Adsorbed FT-IR

Pyridine-adsorbed FT-IR spectra for all samples (Fig. 6) showed characteristic bands at around 1460, 1540 and 1490 cm^{-1}, assignable to pyridine interacting with Lewis (L), Brönsted (B), and B+L acid sites, respectively [38]. The increasing order of the acid amounts was HZM-C16 > HZM-C12 > HZM-C14 > HZM-C10 > ZSM-5 > AT-ZSM-5 for L acid sites, HZM-C12 > HZM-C14 > HZM-C16 > ZSM-5 > HZM-C-10 > AT-ZSM-5 for B acid sites and HZM-C16 ≈ HZM-C14 ≈ HZM-C12 > ZSM-5 > HZM-C-10 > AT-ZSM-5 for the total acid sites. Here, it was worth noting that the amounts of the total acid sites were strongly dependent on the probe molecules used in the measurement. ZSM-5 presented a lower amount of acid than HZM-C16, HZM-C14 and HZM-C12 by pyridine-IR, but higher by NH_3-TPD. It might be due to the reason that HZMs possessed high accessibility of acid sites resulted from their large amount of mesopores. However, ZSM-5 possessed only micropores. It is expected that pyridine molecules (kinetic diameter 0.58 nm) have a higher mass transfer restriction in the micropore channels of ZSM-5 than NH_3 molecules (kinetic diameter 0.26 nm), and thus a lower amount of acid sites was detected by IR than by TPD measurements. This was further confirmed by the results shown in Fig. 6b, where 2,4,6-trimethylpyridine-adsorbed FT-IR spectra (TMPy-IR) of HZM-C16 and ZSM-5 were displayed: the intensity of all bands for HZM-C16 was much stronger than that for ZSM-5 and no L acid sites were observed in the case of ZSM-5. Koo et al. [39] investigated the acid site distributions on the internal and external surface of carbon-templated mesoporous ZSM-5 zeolites synthesized by microwave and conventional hydrothermal methods using FT-IR spectroscopy with pyridine and 2,6-di-tert-butylpyridine (DTBPy) as probe molecules. In the case of DTBPy (kinetic diameter 1.05 nm), only acid sites located at the external surface of medium pore zeolites were evaluated. Herein, our results obtained with TMPy (kinetic diameter 0.74 nm) as probe molecules are similar to Koo's, i.e. TMPy molecules are too bulky to access to the micropore channels of ZSM-5, so that they only interacted with those acid sites located at the external surface and pore mouth of ZSM-5, inducing the decrease in the adsorption amount. It is indicative of the low accessibility of acid sites in ZSM-5.

3.7 Catalytic Cracking Test

Figure 8 shows the conversion of *n*-dodecane catalytic cracking over ZSM-5, AT-ZSM-5 and ZSM-5/MCM-41 composite zeolite coatings as a function of time on stream (TOS). ZSM-5/MCM-41 composite zeolites and AT-ZSM-5 exhibited different catalytic behaviors from the untreated ZSM-5. The HZMs gave higher conversion of *n*-dodecane than ZSM-5, while AT-ZSM-5 gave an opposite result. Apparently, the high catalytic activity of HZMs was mainly due to their high accessibility of acid sites. The low activity of AT-ZSM-5 might be ascribed to the excessive decrease in the amount of acid sites, which showed the least value by both pyridine-IR and NH_3-TPD, although mesopores were also formed in its crystals during alkaline treatment. Seo and co-workers [19] studied the catalytic cracking of *n*-octane over alkali-treated MFI zeolites and found that alkali treatment on the MFI zeolites led to the reduction of cracking activity because of the loss of acid sites, which was the predominant factor in determining the conversion level. For the four HZM samples, the catalytic activity increased with increasing the size of mesopores, although HZM-C12, HZM-C14 and HZM-C16 had a close amount of total acid sites. Launay et al. [40], Serrano et al. [30] and García et al. [41] found that the catalytic activities of composite materials did not vary monotonously with the amount of acid sites, instead diffusive property also played an important role on the conversion. Prokešová et al. [42] compared the concentrations of B and L acid sites determined by adsorbed d_3-acetonitrile FT-IR spectroscopy and the catalytic activity of nanosized zeolite Beta, pure mesoporous molecular sieve Al-MCM-41 and micro/mesoporous composites prepared by themselves, and commercial zeolite Beta in toluene alkylation, and found that nanosized zeolites possessed a good accessibility of acid sites for the probe molecules and the toluene conversion increased with the decrease in the particle sizes of the catalysts possessing similar acidic properties. Therefore, the authors pointed out that appropriate acid sites together with the decrease in the transport limitations were important to the enhancement of the toluene conversion. Liu et al. [9] investigated the effects of ZSM-5 crystal size (nano- and microscale) on the cracking of *n*-dodecane, and found that the nanoscale HZSM-5 zeolite gave a relatively high and stable conversion of *n*-dodecane compared to the microscale HZM-5 zeolite, and finally concluded that the shorter diffusion path lengths of the reactants may be the major reason for the better catalytic performance of the nanoscale HZM-5 zeolite. Therefore, it was reasonable to assume that the sizes of channels in zeolites were a crucial factor in affecting the catalytic activity of HZMs. The diffusion limitation in HZMs was weakened as a result of the presence of mesopores, thus inducing the improvement of the catalytic activity. (Fig. 7).

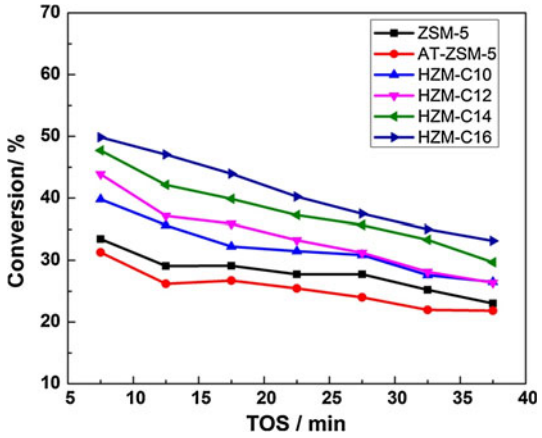

Fig. 7 Conversion versus Time on Stream on different catalyst coatings

TPO data (Fig. 8) provide an indirect evidence of this hypothesis for us. The TPO profiles showed that the amounts of cokes on ZSM-5/MCM-41 composite zeolites decreased as the mesopore size increased. It indicated that the relatively large mesopore was beneficial to the rapid diffusion of cracking products and coke precursors from the channel to surface of zeolites, resulting in lower amount of cokes deposited on the zeolites. Qu et al. [10] investigated the effects of Si/Al ratios of HZSM-5 on the conversion of *n*-dodecane cracking and found that the catalytic cracking activity of HZSM-5 increased gradually with the increase of Si/Al_2 ratios from 25 to 140, although the amount of their acid sites decreased. The authors speculated that the HZSM-5 zeolites with more total acid sites exhibited an abrupt loss of activity in several minutes (less than 5 min) at the beginning of the cracking reaction because of the pore mouth plugging caused by cokes due to

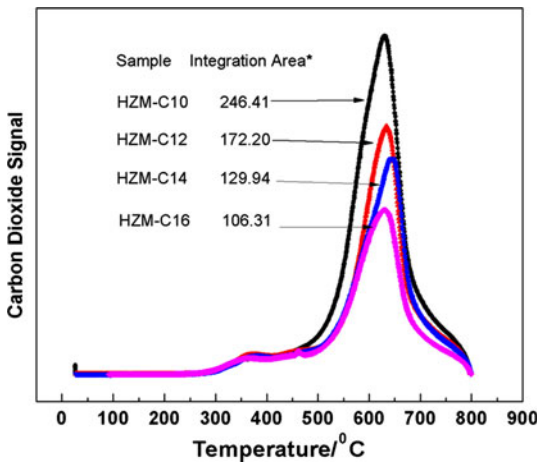

Fig. 8 TPO profiles of cokes over HZM series. Integration Area* was calculated using Gauss-Assisted Software

the high initial catalytic activity. Therefore, the relatively high catalytic activity of the ZSM-5/MCM-41 zeolites with larger mesopores may be the result of the higher diffusivity of reactants and products.

4 Conclusions

The ZSM-5/MCM-41 composite zeolites with the dual-model structures of micropores and mesopores were prepared by desilication and surfactant-directed recrystallization process. The recrystallization was beneficial to the formation of regular mesopores with the pore sizes in the resulting composite zeolites could be controlled by varying the chain length of alkylmethylammonium surfactants. In addition, the recrystallization had a positive effect on the incorporation of Al species dissolved during alkali treatment into zeolite framework, avoiding excess loss of the amount of acid sites. Because of the presence of mesopores, the acid site accessibility and diffusivity of ZSM-5/MCM-41 composite zeolites were improved appreciably. As a result, the ZSM-5/MCM-41 composite zeolites exhibited higher catalytic activity in *n*-dodecane cracking than the untreated ZSM-5 and NaOH-treated ZSM-5 zeolite (without recrystallization) and their catalytic activity continuously increased with the sizes of mesopores.

Acknowledgments Financial support from the National Natural Science Foundation of China (Grants U1232134) is gratefully acknowledged.

Open Access This article is distributed under the terms of the Creative Commons Attribution License which permits any use, distribution, and reproduction in any medium, provided the original author(s) and the source are credited.

References

1. Huang H, Spadaccini LJ, Sobel DR (2004) J Eng Gas Turbines Power 126:284
2. Edwards T (2006) Combust Sci Technol 178:307
3. Meng F, Liu GZ, Qu SD, Wang L, Zhang XW, Mi ZD (2010) Ind Eng Chem Res 49:8977
4. Araújo AS, Fernandes VJ, Araujo SA, Ionashiro M (2002) Nano Mater 141:473
5. Xian XC, Liu GZ, Zhang XW, Wang L, Mi ZT (2010) Chem Eng Sci 65:5588
6. Sobel DR, Spadaccini LJ (1997) J Eng Gas Turbines Power 119:344
7. Sicard MG, Raepsaet B, Ser F (2008) 15th AIAA International space planes and hypersonic systems and technologies conference AIAA p 2008
8. Fan X, Zhong F, Yu G, Li J, Sung C (2009) J Propul Power 25:1226
9. Liu GZ, Zhao GL, Meng FX, Qu SD, Wang L, Zhang XW (2011) Energ Fuel 26:1220
10. Qu SD, Liu GZ, Meng FX, Wang L, Zhang XW (2011) Energy Fuel 25:2808
11. Pérez-Ramírez JC, Christensen CH, Egeblad K, Groen JC (2008) Chem Soc Rev 37:2530
12. Čejka J, Mintova S (2007) Catal Rev 49:457
13. Prokešová P, Mintova S, Čejka J, Bein T (2003) Micro Meso Mater 64:165
14. Groen JC, Bach T, Ziese U, Donk A, Jong K, Moulijin J, Pérez-Ramírez J (2005) J Am Chem Soc 127:10792
15. Groen JC, Peffer L, Moulijin J, Pérez-Ramírez J (2004) Micro Meso Mater 69:29
16. Groen JC, Jansen JC, Moulijin J, Pérez-Ramírez J (2004) J Phys Chem B 108:13062
17. Groen JC, Moulijn JA, Pérez-Ramírez J (2006) J Mater Chem 16:2121
18. Ogura M, Shinomiya SY, Tateno J, Nara Y, Nomura M, Kikuchi E, Matsukata M (2001) Appl Catal A Gen 219:33
19. Jung JS, Park JW, Seo G (2005) Appl Catal A Gen 288:149
20. Zhao L, Gao JS, Xu C, Shen BJ (2011) Fuel Process Technol 92:414
21. Pérez-Ramírez J, Verboekend D, Bonilla A, Abelló S (2009) Adv Funct Mater 19:3972
22. Goto Y, Fukushima Y, Ogura M, Matsukata M (2002) J Porous Mater 9:43
23. Qi J, Zhao TB, Li F, Sun G (2010) J Porous Mater 17:177
24. Han Y, Pitukmanorom P, Zhao L, Ying J (2011) Small 7:326
25. Qian XF, Li B, Hu Y, Niu GX, Zhang D, Che R, Tang Y, Su D, Asiri A, Zhao DY (2011) Chem Eur J 18:931
26. Yoo WC, Zhang X, Tsapatsis M, Stein A (2012) Micro Meso Mater 149:147
27. Meng FX, Liu GZ, Wang L, Qu SD, Zhang XW, Mi ZD (2010) Energy Fuel 24:2848
28. Wang S, Dou T, Li YP, Zhang Y, Li X, Yan Z (2005) Catal Commun 6:87
29. Tang Q, Xu H, Zheng Y, Wang J, Li H, Zhang J (2012) Appl Catal A Gen 413–414:36
30. Serrano DP, García RA, Vicente G, Linares M, Procházková D, Čejka J (2011) J Catal 279:366
31. Cui J, Yang YH, Li Y (1997) Acta Chem Sin 55:974
32. Kokotailo GT, Rohrman Jr AC (1987) US Patents 4,703,025, 27 Oct 1987
33. Mokrzycki Ł, Sulikowski B, Olejniczak Z (2009) Catal Lett 127:296
34. Beck JS, Vartuli JC, Roth WJ, Leonowicz ME, Kresge CT, Schmitt KD, Chu CTW, Olson DH, Sheppard EW, McCullen SB, Higgins J (1992) J Am Chem Soc 114:10834
35. Kresge CT, Leonowicz ME, Roth WJ, Vartuli JC, Beck JS (1992) Nature 359:710
36. Verboekend D, Mitchell S, Milina M, Groen JC, Pérez-Ramírez J (2011) J Phys Chem C 115:14193
37. Groen JC, Moulijn JA, Pérez-Ramírez J (2007) Ind Eng Chem Res 46:4193
38. Li Y, Zhang W, Zhang L, Yang Q, Wei Z, Feng Z, Li C (2004) J Phys Chem B 108:9739
39. Koo JB, Jiang N, Saravanamurugan S, Bejblová M, Musilová Z, Čejka J, Park SE (2010) J Catal 276:327
40. Habib S, Launay F, Laforge S, Comparot JD, Faust AC, Millot Y, Onfroy T, Montouillout V, Magnoux P, Paillaud JL, Gédéon A (2008) Appl Catal A Gen 344:61
41. García RA, Serrano DP, Otero D (2005) J Anal Appl Pyrol 74:379
42. Prokešová P, Žilková N, Mintova S, Bein T, Čejka J (2005) Appl Catal A Gen 281:85